



**HAL**  
open science

# Temporal and Spatial Variability of the Electron Environment at the Orbit of Ganymede as Observed by Juno

S. Pelcener, Nicolas André, Q. Nénon, J. Rabia, M. Rojo, A. Kamran, Michel Blanc, P. Louarn, E. Penou, D. Santos-Costa, et al.

► **To cite this version:**

S. Pelcener, Nicolas André, Q. Nénon, J. Rabia, M. Rojo, et al.. Temporal and Spatial Variability of the Electron Environment at the Orbit of Ganymede as Observed by Juno. *Journal of Geophysical Research Space Physics*, 2024, 129 (5), 10.1029/2023JA032043 . hal-04792026

**HAL Id: hal-04792026**

**<https://hal.science/hal-04792026v1>**

Submitted on 20 Nov 2024

**HAL** is a multi-disciplinary open access archive for the deposit and dissemination of scientific research documents, whether they are published or not. The documents may come from teaching and research institutions in France or abroad, or from public or private research centers.

L'archive ouverte pluridisciplinaire **HAL**, est destinée au dépôt et à la diffusion de documents scientifiques de niveau recherche, publiés ou non, émanant des établissements d'enseignement et de recherche français ou étrangers, des laboratoires publics ou privés.



Distributed under a Creative Commons Attribution - NonCommercial - NoDerivatives 4.0 International License

# JGR Space Physics

## RESEARCH ARTICLE

10.1029/2023JA032043

### Key Points:

- We present composite electron energy spectra combining all Juno particle data from 07/2017 to 08/2022 at Ganymede's orbit
- We study the variability of electron fluxes inside and outside the Jovian magnetodisk as well as within Ganymede's magnetosphere
- Galileo-based models underestimate the electron fluxes observed by Juno in particular at high energies

### Correspondence to:

N. André,  
nicolas.andre@irap.omp.eu

### Citation:




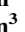
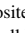






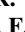


Pelcener, S., André, N., Nénon, Q., Rabia, J., Rojo, M., Kamran, A., et al. (2024). Temporal and spatial variability of the electron environment at the orbit of Ganymede as observed by Juno. *Journal of Geophysical Research: Space Physics*, 129, e2023JA032043. <https://doi.org/10.1029/2023JA032043>

Received 1 SEP 2023  
Accepted 20 APR 2024

© 2024. The Authors.

This is an open access article under the terms of the [Creative Commons Attribution-NonCommercial-NoDerivs License](#), which permits use and distribution in any medium, provided the original work is properly cited, the use is non-commercial and no modifications or adaptations are made.

## Temporal and Spatial Variability of the Electron Environment at the Orbit of Ganymede as Observed by Juno

S. Pelcener<sup>1</sup>, N. André<sup>1,2</sup> , Q. Nénon<sup>1</sup>, J. Rabia<sup>1</sup> , M. Rojo<sup>1</sup>, A. Kamran<sup>1</sup> , M. Blanc<sup>1</sup> , P. Louarn<sup>1</sup> , E. Penou<sup>1</sup>, D. Santos-Costa<sup>3</sup>, F. Allegrini<sup>3</sup> , R. W. Ebert<sup>3,4</sup> , R. J. Wilson<sup>5</sup> , J. Szalay<sup>6</sup> , B. H. Mauk<sup>7</sup> , C. Paranicas<sup>7</sup> , G. Clark<sup>7</sup> , F. Bagenal<sup>5</sup> , and S. Bolton<sup>3</sup> 

<sup>1</sup>IRAP, CNRS-UPS-CNES, Toulouse, France, <sup>2</sup>Institut Supérieur de l'Aéronautique et de l'Espace (ISAE-SUPAERO), Université de Toulouse, Toulouse, France, <sup>3</sup>SwRI, San Antonio, TX, USA, <sup>4</sup>University of Texas at San Antonio, San Antonio, TX, USA, <sup>5</sup>Laboratory for Atmospheric and Space Physics, Boulder, CO, USA, <sup>6</sup>Princeton University, Princeton, NJ, USA, <sup>7</sup>APL, Johns Hopkins University, Laurel, MD, USA

**Abstract** The thermal and energetic electrons along Ganymede's orbit not only weather the surface of the icy moon, but also represent a major threat to spacecraft. In this article, we rely on Juno plasma measurements to characterize the temporal and spatial variability of the electron environment upstream of Ganymede. In particular, we find that electron spectra observed by Juno have fluxes larger by a factor of 2–9 at energies above 10 keV than what was measured two decades earlier by Galileo. This result will advance our understanding of the surface weathering and may be a concern for the radiation safety of the JUICE mission. Furthermore, the June 2021 close fly-by of Ganymede through the moon's wake reveals that the open field line regions of its magnetosphere attenuate electron fluxes at all energies by a factor of 1.6–5, thereby offering a natural shelter to visiting spacecraft crossing this region.

**Plain Language Summary** Ganymede, the only magnetized moon in our Solar System, orbits deep inside the giant magnetosphere of Jupiter where it interacts with the temporally and spatially variable magnetized disk of plasma in corotation around the planet, its magnetodisk. The intensities of ions and electrons precipitating to the surface of Ganymede in particular depend on the location of the moon with respect to the Jovian magnetodisk. In this work, we provide a full quantification of electron properties along the orbit of Ganymede as observed by Juno. This is done by combining observations from two instruments in order to build composite electron energy spectra and derive their omnidirectional fluxes, densities, and pressures. We report that the average electron omnidirectional fluxes are significantly attenuated when measured above or below the magnetodisk, as well as strongly inside the magnetosphere of the moon where its intrinsic magnetic field provides additional shielding. We confirm that the electron total density is dominated by the thermal population, whereas the total pressure is dominated by the suprathermal one. When comparing our results with Galileo-based observations and models, we find that the latter two underestimate fluxes in particular at high energies, and we put these observations in context for the future exploration of Ganymede by JUICE.

## 1. Introduction

Ganymede is the largest moon in our solar system and the only moon known to possess an intrinsic magnetic field. The interaction of the magnetic field, ionosphere, and subsurface ocean of Ganymede with the magnetized, sub-Alfvénic, subsonic, Jovian plasma results in a mini-magnetosphere around the Galilean moon. Since Ganymede orbits near the edge of Jupiter's most intense radiation belts (Evans et al., 2013), it is constantly bombarded by trapped electrons and ions that precipitate, impact, and alter the properties of its surface. Electrons in particular play an important role in modifying the structural, optical, and thermal properties of the surface (Baragiola, 2003; Cooper et al., 2001; Schaible et al., 2017). Observed albedo differences have been found correlated with the magnetic field configuration near the moon, leading to asymmetries between polar and equatorial regions as well as between the trailing and leading hemispheres (Khurana et al., 2007). Electron weathering of the poles of Ganymede has recently been related to the formation of peroxide observed there (Trumbo et al., 2023).

The upstream electron distribution informs on the state of the Jovian magnetosphere and governs the Ganymede-magnetosphere interaction (Fatemi et al., 2016; Liuzzo et al., 2020; Plainaki et al., 2015; Poppe et al., 2018), electron precipitation to the surface (e.g., Liuzzo et al., 2020), and ionization of the moon exosphere (e.g., Vorburger et al., 2022; Leblanc et al., 2017, 2023). Whereas both short- and long-term dynamics as well as

latitudinal, longitudinal, M-shell, and local time variability of the Jovian magnetic field and plasma at the orbit of Ganymede have been previously reported (Bagenal et al., 2016; Jun et al., 2005; Krupp et al., 2004; Mauk et al., 1999, 2020; Vogt et al., 2022), the impact of this variability for incident charged particle fluxes has however not been fully explored in those previous studies. Paranicas et al. (2021) recently reported electron differential fluxes measured by Juno (Bolton et al., 2017) near Ganymede's orbital distance significantly higher than previously considered, although they acknowledged that their study only provided a single snapshot of the prevailing plasma and energetic particle conditions there at the time of their measurements.

The objective of this paper is therefore to provide a more complete characterization and quantification of the temporally and spatially variable electron environment at the distance of Ganymede's orbit. This is of prime importance for both surface, exosphere, and magnetosphere modeling and measurements, as well as for the radiation environment encountered by spacecraft in orbit around Ganymede like the Jupiter Icy Moons Explorer (JUICE) of the European Space Agency (ESA).

This paper is organized as follows: Section 2 details the method applied and data used in order to derive composite electron spectra and moments in the Jovian magnetosphere from Juno multi-instrument observations. Section 3 summarizes the spatially and temporally variable properties of electron populations observed at the distance of Ganymede's orbit, and compares/contrasts our new Juno observations with those from past missions as well as with predictions from various empirical models of the Jovian electron populations. Section 4 concludes our study.

## 2. Instrument Description and Methodology

### 2.1. Searching for the Time Periods When Juno Crossed the Environment Where Ganymede Orbits

Ganymede orbits Jupiter at a joviocentric radial distance of  $15 (\pm 0.1) R_J$ , where  $1 R_J$  corresponds to one equatorial planetary radius and equals to 71,492 km. During its orbit the magnetic latitude of the moon varies from  $-10^\circ$  to  $10^\circ$ . We first identify all time periods when Juno crossed the environment where Ganymede orbits by constraining the radial distance of the spacecraft to be between  $14$  and  $16 R_J$  and its magnetic latitude to vary from  $-11^\circ$  to  $11^\circ$ . Our conditional search applied between July 2017 (PeriJove (PJ) PJ7) and April 2023 (PJ50) initially resulted in a catalog of 43 time intervals with duration ranging between 10 and 180 min.

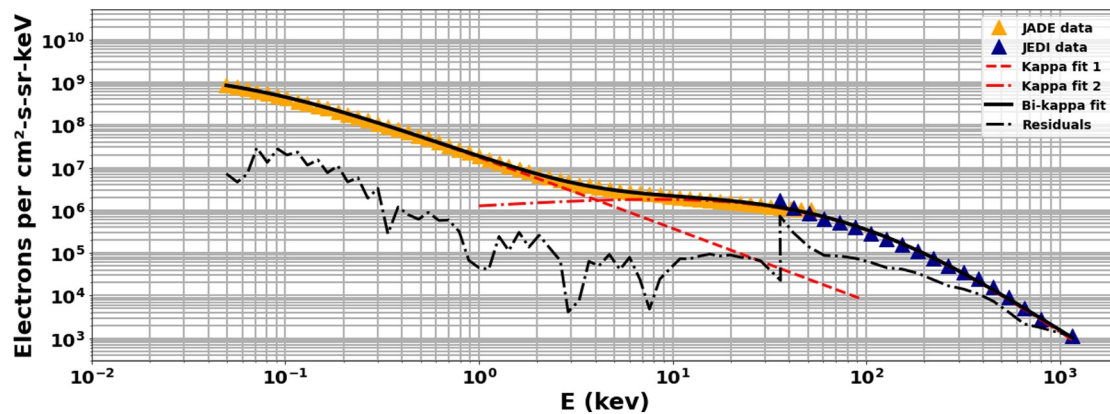
### 2.2. Combining Observations From the JADE and JEDI Instruments

For each time interval identified in our catalog we then looked at in situ 1 and 0.5 s resolution electron data obtained by the Jupiter Auroral Distribution Experiment (JADE, McComas et al., 2017) and the Jupiter Energetic Particle Detector Instrument (JEDI, Mauk et al., 2017) onboard Juno, respectively. We combined JADE and JEDI measurements in order to obtain composite energy spectra of electrons over the full JADE plus JEDI energy range as JADE observes electrons from 100 eV to 100 keV, 50 eV to 100 keV, and 32 eV to 32 keV, and JEDI observes 30 keV to 1 MeV electrons using measurements pixilated into small and large pixels with different sensitivities during the different time intervals within the time period used. The JADE-E electron sensors consist of two identical electrostatic analyzers with a  $120^\circ$  field of view in spacecraft azimuth, JADE-E060 and JADE-E180. The three electron detectors The three high-energy electron detectors, JEDI-90, JEDI-180, and JEDI-270, each consist of six different telescopes that are looking at different directions. The JEDI-90 and JEDI-270 sensors view within the horizontal plane of Juno, while the JEDI-180 sensor views perpendicular to the equatorial plane of the spacecraft. All the electron sensors of JADE and JEDI combined with the 30 s spin of Juno allows a good coverage ( $>130^\circ$ ) in the pitch angle domain depending on the orientation of the spacecraft. The availability of simultaneous JADE and JEDI observations for each of the time intervals of our catalog led to a reduction from 43 to 35 useable cases.

### 2.3. Intercalibration of the JADE and JEDI Omnidirectional Electron Fluxes

The JADE and JEDI monodirectional fluxes  $F$  are taken from the Planetary Data System (PDS, see Data Availability section) and combined into omnidirectional electron fluxes  $j_e$  using

$$j_e = \sum_i F_i \times \sin(\alpha_i) \times (\alpha_{i+1} - \alpha_i), \quad (1)$$



**Figure 1.** Composite electron energy spectrum for one of the time interval in our catalog (15 September 2020, 09:55–11:05 UT). The JADE and JEDI omnidirectional fluxes are displayed using orange and blue triangles, respectively. The red dashed and dash-dotted lines correspond to the first and second term of the bi-kappa distribution covering JADE and JEDI energies, respectively. The black solid line corresponds to the bi-kappa distribution given by Equation 2 when the two terms are summed. The black dash-dotted line represents the absolute value of the difference between the observations and the bi-kappa fit.

with  $\alpha_i$  the pitch angles associated to each JADE or JEDI looking directions  $i$ . As described in the Supporting Information of Mauk et al. (2017, 2023), PDS electron fluxes early in the mission have not been corrected the minimum ionization effect for the detection efficiency of high-energy electrons, while those later in the mission include the correction introduced by Mauk et al. (2017). In addition, Paranicas et al. (2022), their Figure 2, showed raw versus electron data corrected for minimum ionization effect at Ganymede and this only amounts to (at most) a factor of 2 issue. Therefore we will ignore this additional correction here. Moreover, we are aware of the highly dynamic aspect of the magnetosphere where Ganymede orbits. Interchange events are frequently observed in that region, where the cold and dense plasma originating from Io moves from the inside to the outside of the magnetosphere, while the warm and lower density plasma from the outer magnetosphere moves inward (Achilleos et al., 2015). Mauk et al. (1999) have shown that injection events with highly variable fluxes of charged particles are also observed in the region of interest here. These events can last a long time and merge with follow-on injections, adding significant complexities to the characterization of the charged particle environment encountered at the distance of Ganymede's orbit. However, we noticed that when observed in our catalog such interchange/injection events are short lived, and represented only a small fraction of our time intervals considered (less than 10%). It is consistent with previous observations so we didn't remove their time periods of our calculations when they were observed since they can be neglected. In addition, our time intervals did not encompass any of the large-scale energetic electron injections with a characteristic time scale of one hour as reported by Mauk et al. (1999) and Haggerty et al. (2019). However, we acknowledge that we may not have been able to see such a large injection event if it would have started before the start of one of our time interval.

Figure 1 displays the resulting averaged composite electron spectrum for one particular time interval of our catalog. In this particular case as well as in all the other cases, we could identify some slight discrepancies for a limited number of energies where the JADE and JEDI data sets overlap, mainly due either to the reduced efficiency of the Solid-State Detectors (SSD) of JEDI in its low-energy range, or to penetrating particles measured by JADE in its high-energy range, or to the different response functions of these instruments at these overlapping energies. Concerning the discrepancies of JEDI, we noticed interesting changes in pattern through time, with higher counts observed at low energies on each energy spectra until PJ 19, then lower ones until PJ 36, and finally both higher and lower ones mixed on each energy spectra for the rest of the PJ. In the rest of our analysis we did not include these energies (typically the last five energies of JADE and the energies below 30 keV for JEDI), as done by Paranicas et al. (2021).

There were also a few discarded cases where the JADE and JEDI data sets did not match significantly. Overall, JADE and JEDI provided similar fluxes in their overlapping range for 73% of the time intervals included in our catalog. This resulted in a final workable catalog reduced to 27 time intervals, from PJ10 to PJ44. Our catalog does not include any events prior to the end of 2017 since Juno crossed the equatorial magnetosphere farther out from the distance of Ganymede's orbit. Juno was not in the range of radial distances and magnetic latitudes used in our conditional search.

#### 2.4. Modeling of the Observed Electron Populations With Bi-Kappa Distribution Functions

Since Voyager it is known that the plasma trapped by Jupiter's magnetic field is composed of different electron populations in the energy range covered by JADE and JEDI (Krimigis et al., 1981; Scudder et al., 1981), including the low-energy thermal component of the magnetospheric plasma below 100s eV, the keV suprathermal hot electrons, and the high-energy tail extending into the MeV energy range as at Saturn (van Allen, 1979). In order to determine the electron distribution functions from our composite electron spectra, we relied on an extended kappa distribution introduced in Hawkins III et al. (1998) which is known to fit better the extended tails of the magnetospheric plasmas:

$$j_e = j_1 \left( \frac{E}{E_1} \right)^{\gamma_1} \left( 1 + \frac{E}{E_1} \right)^{-\gamma_1 - \kappa_1} + j_2 \left( \frac{E}{E_2} \right)^{\gamma_2} \left( 1 + \frac{E}{E_2} \right)^{-\gamma_2 - \kappa_2}, \quad (2)$$

where  $j$  are electrons per  $\text{cm}^2\text{-s-sr-keV}$ ,  $E$  are energies in keV, and  $\kappa$  and  $\gamma$  are invariant indices. The first term of the right-hand side of Equation 2 mainly covers the JADE energy range whereas the second term of the right-hand side of Equation 2 mainly covers the JEDI energy range. In order to estimate the eight governing parameters of Equation 2 we followed exactly the method detailed in Paranicas et al. (2021). Figure 1 illustrates the well-fitness of the data and our bi-kappa model with  $j_1 = 4e9 \text{ cm}^2\text{-s-sr-keV}$ ,  $E_1 = 0.043 \text{ keV}$ ,  $\gamma_1 = 0.4$ , and  $\kappa_1 = 1.7$ ,  $j_2 = 5e6 \text{ cm}^2\text{-s-sr-keV}$ ,  $E_2 = 85 \text{ keV}$ ,  $\gamma_2 = 0.3$ , and  $\kappa_2 = 3.2$  for one of the time interval in our catalog, with residuals ranging between 10% and 20% of the observations.

#### 2.5. Determination of the Position of Juno Relative to the Jovian Magnetodisk

Jupiter's magnetic field is tilted by about  $10^\circ$  with respect to the planet's spin axis, and this implies that along its orbit Ganymede is either embedded within the magnetodisk of Jupiter, or above it, or below it. Depending on these three different configurations, the electron spectra differ and this results in different intensities for the electron bombardment of Ganymede's surface. Therefore, it is necessary to determine the region encountered by Juno for each of the time interval included in our catalog. In order to do this, we modeled the scale height ( $H$ ) of the plasma using the following formula taken from Bagenal and Delamere (2011):

$$h = a_1 + a_2 r + a_3 r^2 + a_4 r^3 + a_5 r^4, \quad (3)$$

with  $h = \log_{10}(H)$  and  $r = \log_{10}(R)$ , and  $R$  the jovigraphic radial distance normalized to Io's radial distance ( $6 R_J$ ). The  $a_1, a_2, a_3, a_4$ , and  $a_5$  coefficients are constants equal to  $-0.116, 2.14, -2.05, 0.491$ , and  $0.126$ , respectively. For the orbital constraints considered in our conditional search the plasma scale height varies between  $2.6 R_J$  and  $3 R_J$ . The position of each point of the centrifugal equator at east longitude  $Elon$  is defined by its jovigraphic distance  $R$  and its jovigraphic latitude  $\theta_c$  given by the following formula taken from Phipps and Bagenal (2021):

$$\theta_c(R, Elon) = [a \tanh(b R - c) + d] \sin(Elon - e), \quad (4)$$

The  $a, b, c, d$ , and  $e$  are constants equal to  $1.66^\circ, 0.131^\circ, 1.62^\circ, 7.76^\circ$ , and  $249^\circ$ , respectively. Juno's latitude in a 2D centrifugal frame (assuming  $Elon$  is fixed in  $Z$ ),  $\theta_{cf}$  is given by  $\theta_{cf} = \lambda_{Juno} - \theta_c$  with  $\lambda_{Juno}$  its System III latitude, so that the height of Juno from the centrifugal equator is given by  $R_{Juno} \times \sin(\theta_{cf})$ .

From this, we sorted out our data considering two cases: Case 1 for time intervals when Juno lies within the magnetodisk of Jupiter, and Case 2 for time intervals when Juno is above or below the magnetodisk. In total, this results in 26 time intervals corresponding to 53 hr and 20 min of data cumulated for Case 1, and 6 time intervals corresponding to 1 hr and 25 min for Case 2 with one single time interval corresponding to Juno being below the magnetodisk. Table A1 in Appendix A summarizes the orbital properties for each of the time intervals included in our catalog. All events correspond to different latitudes, longitudes, M-shells, and local time. In particular the latter only varies M-shells covered in our catalog vary between 14.1 and 19.5, whereas the covered local time only vary between 19:00 and 03:30 and, therefore, only a partial coverage in local time is obtained. However, Khurana et al. (2022) reported no significant local time variations for the thickness of the magnetodisk inside  $30 R_J$  and, hence, at the distance of Ganymede's orbit. The local time variations are therefore assumed negligible in the present study.



## 2.6. Derivation of the Electron Density and Pressure

We finally assumed that electron distributions are isotropic at all energies and integrated the observed bi-kappa distributions in energy space in order to estimate their zeroth- and second-orders moments that correspond to the density and pressure, respectively. The reader is referred to Paschmann et al. (1998) for more details. We estimated with two methods the total density and pressure by integrating over the full JADE plus JEDI energy range (a) our observed composite electron spectra, as well as (b) our fitted extended bi-kappa distribution. The two methods gave almost similar values (a 2% difference was observed). In addition, we also estimated the partial density and pressure of the thermal and suprathermal electron populations by integrating separately the first and the second terms of the fitted extended bi-kappa distribution over the JADE energy range and the JEDI energy range, respectively. We did not estimate the temperature of the thermal and suprathermal electron populations since they can easily be obtained by dividing their partial pressure with their partial density. Table B1 in Appendix B summarizes the values for each of the time intervals included in our catalog.

## 3. Results

### 3.1. Spatial and Temporal Variability of Electron Fluxes

The first panel of Figure 2 presents the energy spectra of the omnidirectional electron fluxes accumulated during all the time intervals of Table A1 far upstream of Ganymede. Measurements in the magnetodisk (Case 1) and above it (Case 2) are shown in pink and gray, respectively. The second and third panels of Figure 2 detail the measurements for Case 1 and Case 2 only, respectively, together with the corresponding averages of all electron omnidirectional fluxes measured in those regions. The fourth panel summarizes the average fluxes for Case 1 (in red) and Case 2 (in black), together with the average flux along one complete (7.15 days) orbit of Ganymede around Jupiter (in green). The latter is calculated considering that during its orbit Ganymede is approximately 55% of the time outside the magnetodisk, and 45% within it. Table C1 in Appendix C provides the values for the parameters of the bi-kappa distributions fitting the average fluxes presented in this panel.

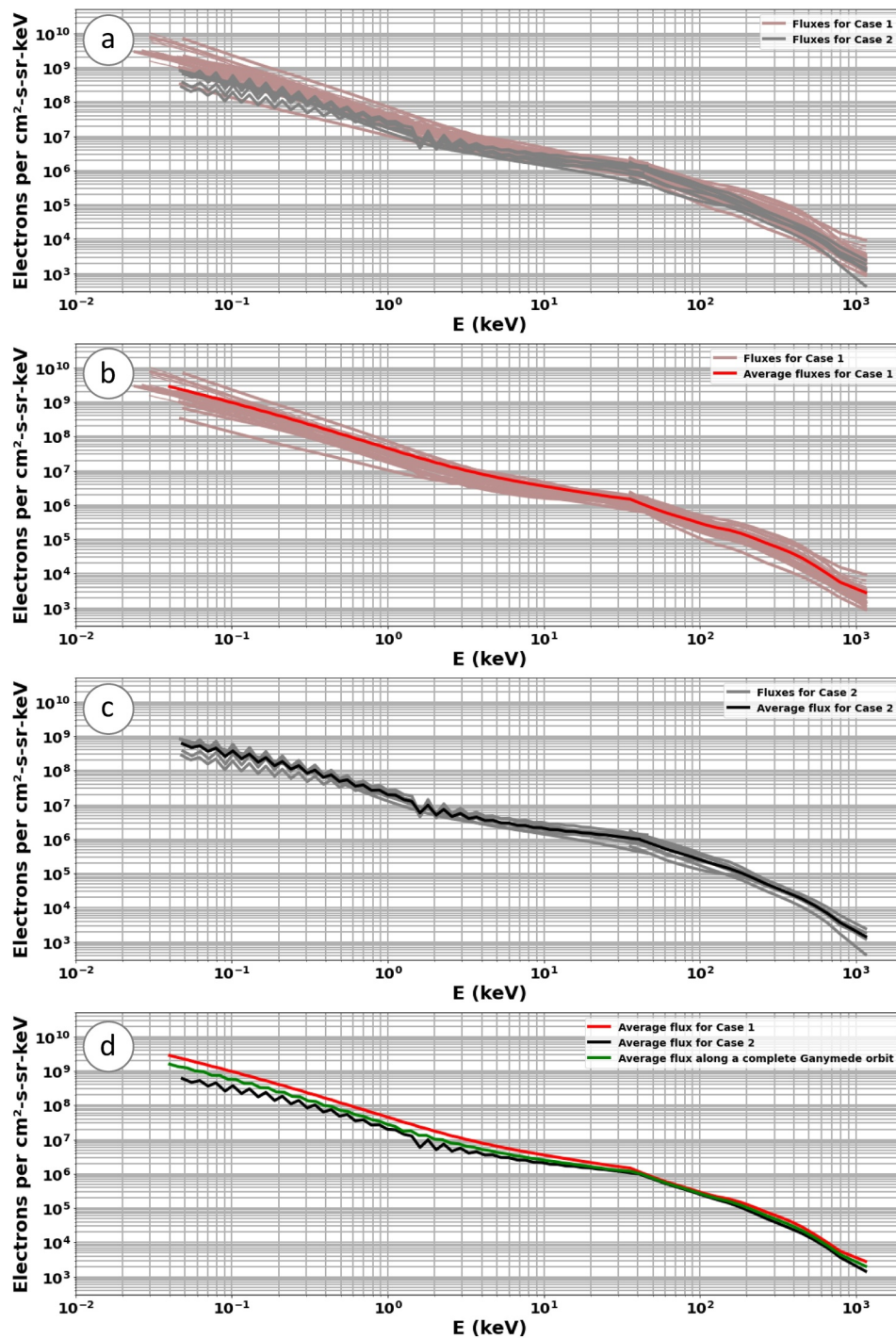
As expected, the first and fourth panels of Figure 2 show that the fluxes of low-energy electrons are higher inside the magnetodisk rather than above it, as expected, by a factor of 3 on average. Energetic electron fluxes exhibit a lower in-and-out difference of a factor of around 1.5. This is consistent with the quasi-isotropic pitch angle distributions of energetic electrons in this region (Ma et al., 2021; Nénon et al., 2022; Tomás et al., 2004). Whereas in the JEDI range the 100–500 keV is higher in the magnetodisk, this is also where MeV electrons contribute to the signal, so we will need to investigate this further in a future study. Figure 2 also reveals a clear variability of electron spectra from one crossing of the orbit of Ganymede to another. At the highest energies observed by JEDI, this variability reaches an amplitude of a factor of 10, consistent with the time variability observed by Galileo for MeV electrons (Jun et al., 2005). We also note a variability of a factor of 10 for the lowest-energy electrons. Suprathermal electrons in the energy range of 5–30 keV may have a less pronounced variability (factor of 3) than the other energies.

Figure 2 shows that electron fluxes are on average less intense when located outside the magnetodisk. This result is not really surprising, but what is interesting is that there seems to be a greater difference for low-energy electrons in the JADE data.

On average, there are 3.2 times more low-energy electrons in the magnetodisk plasma than above. For high-energy electrons, the difference is significantly less, with an average factor of 1.5. There is also a fairly large temporal variation in the fluxes of high-energy electrons, for instance if we focus on the individual fluxes encountered in the magnetodisk we can see a factor of an order 10 on the second panel of Figure 2. These variabilities are even more important since they are never taken into account in simulations of Ganymede's magnetosphere. Then, we computed and characterized the total and partial electron densities and pressures by assuming the electron fluxes are omnidirectional.

### 3.2. Contributions of the Various Electron Populations to the Plasma Density and Pressure

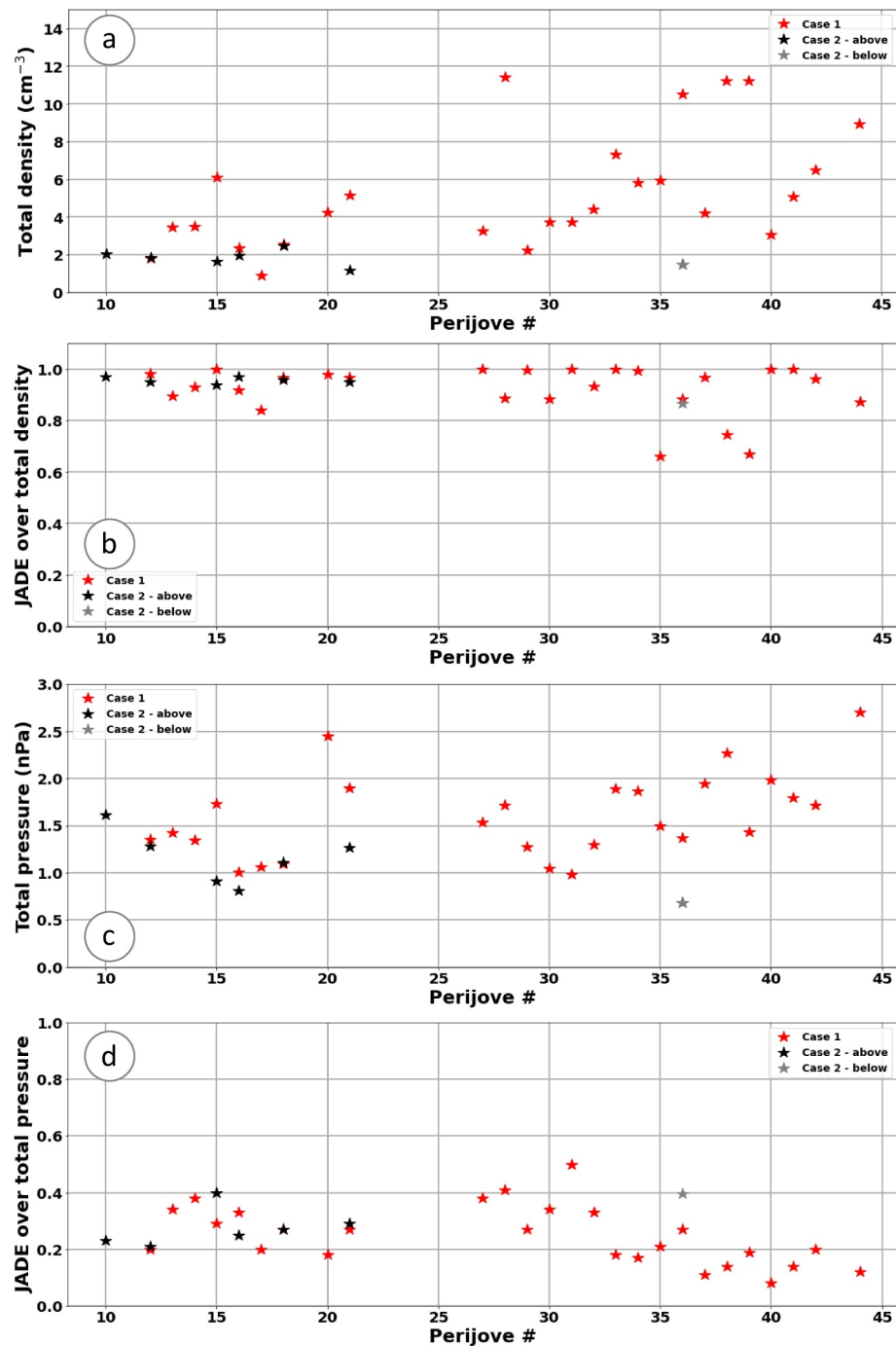
From the method presented in Section 2.6, we calculated for each time interval considered the total electron density and pressure from the omnidirectional electron fluxes and their energy. We decided to study the temporal and spatial variation of these parameters, that is to say their values depending on the height  $z$  of Juno during the



**Figure 2.** First panel: Electron omnidirectional fluxes sorted according to their origin (in pink, those measured inside the magnetodisk corresponding to Case 1; in gray, those measured above it corresponding to Case 2). Second panel: Electron omnidirectional fluxes for Case 1 together with their average (in red). Third panel: Electron omnidirectional fluxes for Case 2 together with their average (in black). Fourth panel: Red represents the average flux measured inside the magnetodisk, black the average flux measured above the magnetodisk, and green the average flux along one complete orbit of Ganymede around Jupiter.

data collection respectively to the height  $H$  of the magnetodisk's plasma, as shown in Figure 3. In this figure, we can also look at the contribution of thermal and suprathermal electron populations in both of these parameters.

In the first and third panels of Figure 3, we can remark that the total electron density and pressure show variability over the 5 years of data taken into account during this study, ranging from 1 to 12 cm<sup>-3</sup> and from 0.6 to 2.9 nPa,



**Figure 3.** First panel: variation of the total electron density (in  $\text{cm}^{-3}$ ) with Perijove number (#). Second panel: same for the density estimated over the JADE energy range and divided by the total density. Third panel: variation of the total electron pressure (in nPa) with Perijove. Fourth panel: same for the pressure estimated over the JADE energy range and divided by the total pressure. Red represents the densities and pressures of electron fluxes in the magnetodisk (Case 1), whereas black and gray represent the densities and pressures for electron fluxes located above and below the magnetodisk (Case 2), respectively.

confirming respectively the work published in Bagenal & Delamere, 2011 (derived from a summation of currents measured across the 10–6000 eV energy range) and Mauk et al. (1996) (derived from energies greater than 200 keV). However, it is important to note that the Juno densities and pressures are calculated from electrons of energies between 0.05 and 1155 keV. Although this energy range is quite large, we must not forget that it may



represent only a part of the population of electrons around Ganymede and anything below the low-energy cutoff of JADE in particular will contribute significantly to the density.

We can also notice in the first and third panels of Figure 3 that the densities and pressures of the electron fluxes encountered in the magnetodisk (in red) are significantly higher than those of the surrounding fluxes (in black and gray). This conclusion is not surprising if we consider the difference in electron fluxes between those encountered in the magnetodisk or not. In addition, the total densities and pressures of electrons below (in gray) or above (in black) the magnetodisk are certainly less important but it can also be noted that they appear to be about equal. Electron populations on both sides of the magnetodisk therefore appear to be similar. However, we have only one case characterizing the lower environment, so it is best to take this analysis cautiously.

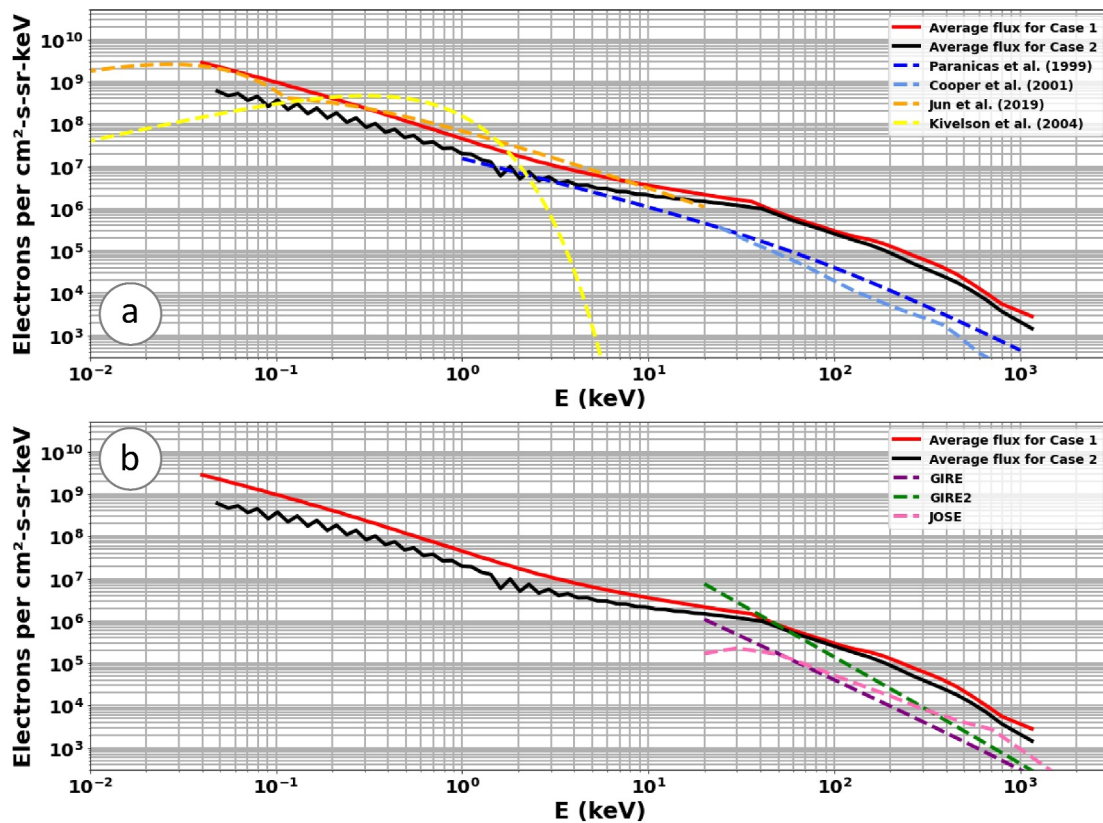
In the second and fourth panels of Figure 3, we can observe the contribution of thermal (observed by JADE) electron populations to the total density and pressure. It seems that the cold electron population still largely dominates the electron density, representing on average more than 93% of the total density. On the other hand, the hot electron population dominates the electron pressure, at a rate of more than 75% of the total pressure with more temporal variation. The work done here on the contribution of the different populations of electrons highlights the need to take into account both populations to completely study the plasma in this region of the Jovian magnetosphere.

### 3.3. Comparison With Galileo-Based Empirical Models and Observations: Implications for the JUICE Mission

We now compare our electron omnidirectional fluxes observed at the time of Juno with Galileo-based observations and models by superimposing the Juno-based average observations displayed in our Figure 2 onto Figure 3 of Liuzzo et al. (2020). Figure 4 is divided into two panels in order to show the results of this comparison. The first panel includes observations (in dark blue) obtained during the G2 and G7 Galileo flybys of Ganymede from the Energetic Particle Detector (EPD, Williams et al., 1992) and PLasma Science (PLS, Frank et al., 1992), as presented in Paranicas et al. (1999), as well as observations (in light blue) obtained during the G2 flyby of Ganymede from EPD, as presented in Cooper et al. (2001). An additional fit (in orange) combining a Maxwellian and kappa distribution is also shown, as presented by Jun et al. (2019). To compare these ambient energetic electron fluxes with the thermal electron population, a fit (in yellow) of a Maxwellian distribution of the ambient plasma near Ganymede is added using average values from Kivelson et al. (2004). The G7 encounter happened at a local time (19:44) covered by some of our Juno events, which makes the comparison directly relevant. This is also probably still valid for the G2 Ganymede flyby, although it happened at a local time (10:45) not covered by any Juno event, since there are no significant local time variations for the thickness of the magnetodisk inside  $30 R_J$  and, hence, at the distance where Ganymede orbits, as reported by Khurana et al. (2022) from magnetic field measurements.

The second panel includes average fluxes near Ganymede's orbit estimated from the GIRE (in purple) and GIRE2 (in green) models, as presented in Garrett et al. (2003), Jun et al. (2019), and de Soria-Santacruz et al. (2016), respectively, as well as from the engineering JOSE model (in pink) developed by Sicard-Piet et al. (2011) and used by ESA in order to design its JUICE mission to Jupiter and Ganymede (Grasset et al., 2013).

First, the quantitative comparison presented in the first panel of Figure 4 shows that the Galileo-based observations and fits seem consistent at low energies with the new Juno-based observations. Both match almost perfectly (orange and red curves) for the case where the moon is embedded within the Jovian magnetodisk, whereas the Galileo-based fluxes are higher than the Juno-based fluxes in the case when the moon is above or below the Jovian magnetodisk (orange and black curves). This may be explained by the fact that the Galileo-based observations and models are mainly representative of the case when the moon is embedded within the Jovian magnetodisk. Second, the Galileo-based observations and models deviate more strongly from the new Juno-based observations at high energies, where they underestimate the fluxes by an average factor of 11, regardless of the various cases considered. At these energies, the second panel of Figure 4 shows that the GIRE2 model remains the closest to the new Juno-based observations (green red, and black curves) but the latest present an harder spectrum. This could be due either to changes in the dynamics and energetic particle content of Jupiter's magnetosphere between the Galileo and Juno epochs, separated in time by 20 years.



**Figure 4.** Electron differential number fluxes reproduced from Figure 3 of Liuzzo et al. (2020) superimposed with our Juno-based average electron omnidirectional fluxes for Case 1 (in red) and Case 2 (in black). First panel: Dark blue represents measurements from Paranicas et al. (1999), light blue represents measurements from Cooper et al. (2001), orange represents a combined Maxwellian and kappa distribution from Jun et al. (2019), and yellow represents a Maxwellian distribution of the ambient plasma near Ganymede from Kivelson et al. (2004). Second panel: Purple, green, and pink represent the average fluxes near Ganymede's orbit estimated by the GIRE, GIRE2, and mean JOSE models, respectively. See text for more details.

We also compared in the second panel of Figure 4 our Juno-based observations with the mean JOSE model (see Table D1 in Appendix D). Again, the model strongly underestimates (pink, red, and black curves), for all the energies they have in common and by a factor ranging from 2 to 9, the observed Juno-based fluxes in the ambient, undisturbed plasma near Ganymede. It is worth mentioning that the observed change in slope or hump in the Juno spectra that begins between about 100 and 400 keV can be due to roughly 1 MeV or greater electrons that fully penetrate the detector. These electrons leave a fraction of their energy in the JEDI SSD detectors, which mimics the energy loss expected for 100–200 keV electrons (Paranicas et al., 2022) and correspond to the minimum ionizing effect of Mauk et al. (2017). As shown in Paranicas et al. (2022), their Figure 2, this contamination only amounts to (at most) a factor of 2 issue at Ganymede, and, therefore, can not explain the more significant difference reported here between the observed Juno-based fluxes and the models. This difference may have important implications in term of signal-to-noise ratio (SNR) for future particle measurements to be obtained by JUICE instruments during its flybys of Ganymede as well as during its orbital phases around the moon. However, during all these phases, JUICE will likely spend a significant part of its time within the magnetosphere of Ganymede where it will encounter a significantly different plasma environment (Allegrini et al., 2022).

### 3.4. Juno's Ganymede Flyby: Estimation of the Shielding Role of the Magnetosphere

Almost 20 years after the end of the Galileo mission, the flyby of Ganymede by Juno on 07 June 2021 offers a unique opportunity to compare the electron omnidirectional fluxes observed inside its mini-magnetosphere to closest approach (1,049 km from the surface) with those observed outside of it. This flyby is included in one time interval in our catalog that corresponds to the case when Juno lies within the magnetodisk. Since Juno crossed different plasma regions during the flyby (Allegrini et al., 2022), we further subdivided this particular time interval into three time sub-intervals: two of them, from 15:25 to 16:50 (interval A) and from 17:05 to 18:15

(interval C), when Juno is outside the magnetosphere of Ganymede, in the ambient, undisturbed Jovian plasma near Ganymede, and a third one from 16:50 to 17:00 (interval B) when Juno is embedded into the open field line regions of the magnetosphere of Ganymede, with an altitude relatively relative to the surface confined between 1,049 and 3,890 km. Allegrini et al. (2022), Valek et al. (2022) and Ebert et al. (2022) reported the JADE measurements during the Ganymede fly-by, while Clark et al. (2022) documented JEDI observations. However, previous authors did not investigate the amplitude of the reduction of electron omnidirectional flux offered by the mini-magnetosphere of Ganymede.

The first and second panels of Figure 5 display the average electron omnidirectional fluxes observed during our three time sub-intervals. The first panel of Figure 4 shows that the properties of the plasma and energetic particles encountered before and after the crossing of the magnetosphere appear similar. The average flux observed during the time sub-intervals when Juno is outside of the magnetosphere of Ganymede agrees remarkably well with the average flux derived in Figure 2 for the case where Juno lies within the magnetodisk of Jupiter (Case 1). This confirms the findings of Vogt et al. (2022) obtained from magnetic field measurements only that the magnetospheric conditions at the time of the flyby were very close to the average. The second panel of Figure 4 shows that a significant reduction in the electron omnidirectional flux at all energies is observed when Juno crossed the moon's wake and is embedded into the open field line regions of the magnetosphere of Ganymede, well below the average flux corresponding to the external conditions and superimposed onto the figure. The observed flux also matches very well the flux predicted for the GCO5000 phase of the JUICE mission (in green, see Table D1 in Appendix D) when the spacecraft will be inserted first into elliptical and then into almost polar 5,000 km altitude orbits around Ganymede. Table C1 in Appendix C provides the values for the parameters of the bi-kappa distribution corresponding to observations obtained during interval B. The third panel of Figure 5 provides a more quantitative estimate of this reduction and gives the ratio of fluxes observed inside versus outside of the magnetosphere of Ganymede during the flyby. The observed energy-dependent reduction factor gives on average 1.6 and 5 times lower electron fluxes in the JADE and JEDI energy ranges inside the magnetosphere of Ganymede, respectively. The JEDI flux reduction is in agreement with previous Galileo fly-by measurements (??) and references therein). Although we acknowledge that our estimated reduction is limited to observations made during a single flyby and for the particular case of a crossing of the moon's wake where the absorption by the moon itself plays undoubtedly a significant role. Particle tracing to see the global precipitation pattern within this open field line region at Juno's altitude will be required for any more quantitative discussion on the observed reduction the reader must be reminded that these observations were interestingly obtained during magnetospheric conditions very close to average conditions when Juno lies within the magnetodisk of Jupiter.

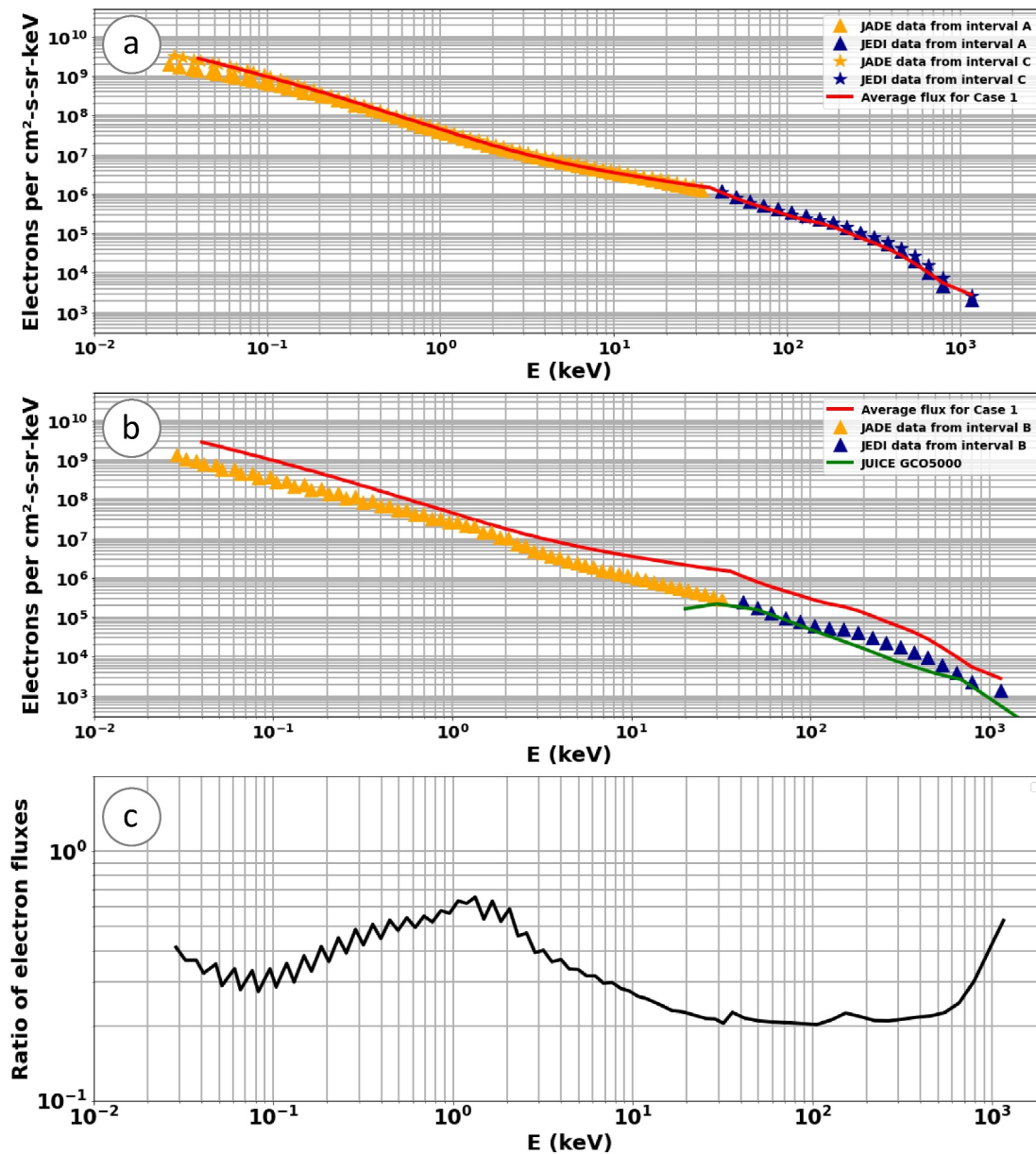
This reduction is of great importance may nevertheless be important in the context of the JUICE mission of ESA that was launched on 14 April 2023. JUICE will become the first spacecraft to orbit another planet's moon, Ganymede, at the end of its mission. During its orbits around Ganymede, as shown in this study, JUICE will regularly cross the moon's wake inside Ganymede's magnetosphere where it will encounter reduced electrons fluxes, and, therefore, benefit from the radiation shielding offered by the moon and its magnetic field (Allioux et al., 2013) in this particular region.

#### 4. Conclusions and Perspectives

The work done here extends the case study published by Paranicas et al. (2021) and makes use of 54 hr of Juno JADE and JEDI measurements obtained over 5 years of the mission in order to characterize the spatial and temporal variability of the electron omnidirectional fluxes, densities, and pressures at the orbit of Ganymede. Our current results are obtained with the best understanding of the instrument responses to date.

In summary:

1. Electron omnidirectional fluxes experience strong energy-dependent temporal variations. The flux of thermal electrons varies by a factor of 24, while that of suprathermal electrons varies by a factor of 10;
2. Electron omnidirectional fluxes experience strong energy-dependent spatial variations whether they are measured within the Jovian magnetodisk, or above, or below it. Within the magnetodisk the flux of thermal and suprathermal electrons are enhanced by a factor 3 and 1.5, respectively;
3. The June 2021 close flyby of Ganymede by Juno reveals that the electron omnidirectional fluxes observed outside of Ganymede's magnetosphere closely match the average fluxes determined for the case when the moon is embedded within the Jovian magnetodisk. The observed fluxes are however strongly reduced at all



**Figure 5.** First panel: Average electron omnidirectional fluxes for intervals A (represented by triangles) and C (represented by crosses) during the Juno's Ganymede flyby when the spacecraft is outside the magnetosphere of Ganymede. JADE data are represented in orange whereas JEDI data are represented in blue. Our average electron omnidirectional flux measured inside the magnetodisk (Case 1) is represented in red. Second panel: Same, for interval B when Juno is embedded within the magnetosphere of Ganymede. The average differential trapped electron fluxes predicted for the JUICE mission during its initial phase in orbit around Ganymede (including its Ganymede Insertion Orbit, elliptical orbits, and circular orbits around Ganymede at an altitude of 5,000 km) is represented in green. Third panel: Average electron omnidirectional fluxes observed during interval B divided by those averaged during intervals A and C.

energies within the open field line regions of Ganymede's magnetosphere through the moon's wake. Whereas the suprathermal electron fluxes are attenuated by a factor of 2.5–5, the thermal electron fluxes are attenuated by a factor of 1.6–3;

4. The total electron density is dominated by the thermal electron population measured by JADE (up to 93%) and ranges from 1 to 12 electrons per cm<sup>-3</sup>. The total electron pressure is dominated by the suprathermal electron population measured by JEDI (up to 75%) and ranges from 0.6 to 2.9 nPa;
5. The comparison of the electron omnidirectional fluxes observed during the Juno mission with Galileo-based observations and models shows a closer agreement at low energies than at high energies where Galileo

- observations are on average 11 times less intense than the fluxes observed by Juno as also noticed by Paranicas et al. (2021) in their very limited sample;
- The comparison of the electron omnidirectional fluxes observed at the time of Juno with the empirical radiation model JOSE used by the European Space Agency for the design of its JUICE mission shows that the latter underestimates by a factor of 2–9 on average the suprathermal electron fluxes between 20 keV and 2 MeV at the distance where Ganymede orbits.

Assuming electrons are isotropic, the electron omnidirectional fluxes observed by Juno where Ganymede orbits are directly proportional within the open magnetic field line region to the fluxes precipitating to the surface of the icy moon Liuzzo et al. (2020); Vorburger et al. (2022). Future studies could use our findings in order to revisit the alteration of Ganymede's surface by precipitating electrons, and address the modifications of its physical, chemical, and optical properties, as done for the ions by, for example, Plainaki et al. (2022). Our results in particular suggest that the surface alteration by electrons with energies greater than 10 keV can be 2 to 9 times greater than estimated in previous studies.

The method developed during this study can be adapted and applied to characterize the electron and ion plasma environments where Galilean moons orbit. Such a detailed characterization will make it possible to constrain input parameters for numerical simulations dedicated to the study of planetary space weather and the moon-magnetosphere interactions at Jupiter, as well as to refine empirical environmental and radiation models at each of them for current and future space missions like JUICE.

## Appendix A: Catalog of Events: Temporal and Spatial Coverage

See Table A1

**Table A1**  
*Start/Stop Time Values for the Orbital Parameters (IAU Latitude in Degree, IAU Longitude in Degree, Local Time in Hour, M-Shell) Corresponding to Particular PJ for Each of the Time Intervals Included in Our Catalog*

Time interval (UT)	PJ #	Latitude (°)	Longitude (°)	Local time (hour)	M-shell
16/12/2017 03:55–04:35	10	17.8/18.3	31.2/7.0	3.3/3.3	16.7/15.3
31/03/2018 17:25–17:55	12	14.0/14.3	295.0/276.9	2.8/2.8	17.0/17.6
31/03/2018 18:00–18:05	12	14.4/14.4	270.9/273.8	2.8/2.8	17.8/18.0
23/05/2018 13:35–16:15	13	13.2/15.3	15.6/278.6	2.5/2.5	16.5/15.4
15/07/2018 12:55–14:55	14	12.1/13.6	341.3/268.6	2.2/2.2	16.2/16.3
06/09/2018 08:55–09:05	15	11.3/11.4	68.1/62.0	1.9/1.9	19.1/18.3
06/09/2018 09:10–11:45	15	11.5/13.5	59.0/325.0	1.9/1.9	17.9/14.2
29/10/2018 07:25–07:35	16	12.4/12.5	63.8/57.8	1.7/1.7	16.1/15.6
29/10/2018 07:40–07:45	16	12.6/12.7	54.7/51.7	1.7/1.7	15.4/15.2
21/12/2018 00:35–00:45	17	9.8/9.9	253.7/247.6	1.4/1.4	17.8/18.3
12/02/2019 03:55–04:05	18	10.7/10.8	74.2/71.2	1.1/1.1	16.1/15.8
28/05/2019 15:45–18:35	20	7.9/10.1	39.5/296.3	0.6/0.6	16.2/14.1
20/07/2019 12:45–12:55	21	8.1/8.3	90.1/84.0	0.4/0.4	18.0/17.3
20/07/2019 13:00–14:30	21	8.3/9.6	81.0/26.3	0.3/0.4	17.0/14.1
01/06/2020 18:05–20:55	27	2.5/4.6	58.5/315.1	22.7/22.7	16.0/14.3
24/07/2020 14:25–16:55	28	2.2/4.1	133.9/45.7	22.5/22.5	18.4/13.9
15/09/2020 09:55–11:05	29	1.3/2.1	239.6/197.1	22.2/22.2	16.1/17.1
07/11/2020 11:15–12:25	30	2.0/2.9	133.5/91.0	22.0/22.0	16.8/14.5
30/12/2020 05:25–08:05	31	0.2/2.1	288.1/191.0	21.8/21.8	16.8/15.9
21/02/2021 01:25–04:15	32	−0.1/2.0	15.7/272.5	21.5/21.6	17.4/14.0



**Table A1**  
*Continued*

Time interval (UT)	PJ #	Latitude (°)	Longitude (°)	Local time (hour)	M-shell
15/04/2021 07:15–10:05	33	−0.7/1.5	106.9/3.7	21.3/21.3	16.5/14.7
07/06/2021 15:25–18:15	34	−1.2/1.0	113.1/9.9	21.0/21.1	16.6/14.7
Time interval (UT)	PJ #	Latitude (°)	Longitude (°)	Local time (hour)	M-shell
07/06/2021 15:25–16:50	34	−1.2/−0.1	113.1/61.6	21.1/21.1	16.6/15.0
07/06/2021 16:50–17:00	34	−0.1/−0.0	61.6/55.5	21.1/21.1	15.0/15.0
07/06/2021 17:05–18:15	34	0.1/1.0	52.5/9.9	21.0/21.1	15.0/14.7
20/07/2021 15:45–18:45	35	−1.9/0.3	109.1/359.8	20.8/20.9	16.4/15.1
02/09/2021 06:15–06:20	36	−2.6/−2.5	310.9/307.9	20.7/20.7	19.5/19.1
02/09/2021 06:20–09:10	36	−2.5/−0.4	307.9/204.7	20.7/20.7	19.1/14.6
16/10/2021 02:15–03:45	37	−2.2/−1.0	313.1/258.5	20.5/20.5	17.5/14.1
28/11/2021 22:35–00:45	38	−3.5/−1.8	303.4/224.6	20.3/20.3	18.6/14.1
11/01/2022 18:55–21:05	39	−4.2/−2.5	293.6/214.8	20.1/20.0	18.3/14.1
24/02/2022 09:35–12:25	40	−5.5/−3.4	129.4/26.3	19.8/19.8	16.1/15.5
09/04/2022 01:15–02:15	41	−5.0/−4.2	288.6/252.1	19.6/19.6	17.1/14.3
22/05/2022 11:35–12:45	42	−6.0/−5.0	281.3/238.9	19.4/19.4	17.2/14.1
16/08/2022 22:35–01:15	44	−8.8/−6.7	257.5/160.5	19.0/18.9	18.3/14.1

*Note.* The time intervals when Juno is within the magnetodisk are indicated in red, whereas the ones when Juno is above or below it are indicated in black and gray, respectively. M-shells are estimated using the JRM33 + CON2020 magnetic field model of Connerney et al. (2022).

## Appendix B: Catalog of Events: Values for the Parameters of the Bi-Kappa Distributions and Electron Moments

See Table B1

**Table B1**

*Values for the Parameters of the Bi-Kappa Distributions Presented in Equation 2 for Each of the Time Intervals Included in Our Catalog*

Time interval (UT)	$j_1/j_2$	$E_1/E_2$	$\gamma_1/\gamma_2$	$\kappa_1/\kappa_2$	$n_e$ (cm <sup>−3</sup> )	$P_e$ (nPa)
16/12/2017 03:55–04:35	1.6e9/7e6	0.06/90	0/0.5	1.5/3.3	2.056	1.612
31/03/2018 17:25–17:55	1.6e9/7e6	0.06/90	0/0.7	1.57/3.3	1.807	1.355
31/03/2018 18:00–18:05	1.6e9/7e6	0.06/90	0/0.65	1.58/3.4	1.853	1.281
23/05/2018 13:35–16:15	1.9e9/4e6	0.05/90	0/0.7	1.2/10	3.467	1.429
15/07/2018 12:55–14:55	2e9/4e6	0.095/90	0/0	1.7/3.3	3.513	1.347
06/09/2018 08:55–09:05	0.8e9/4e6	0.11/60	0.4/0.15	1.5/3	1.636	0.9158
06/09/2018 09:10–11:45	4e9/4e6	0.1/90	0/0.1	1.95/3	5.095	1.732
29/10/2018 07:25–07:35	2.5e9/1.5e6	0.065/70	0.2/0	1.9/2.4	1.958	0.811
29/10/2018 07:40–07:45	1.8e9/2.9e6	0.095/80	0.18/0	1.9/2.9	2.353	1.009
21/12/2018 00:35–00:45	0.5e9/1.6e6	0.048/80	0/0	1.3/2.5	0.907	1.065
12/02/2019 03:55–04:05	3e9/1.6e6	0.06/95	0.5/0	1.7/2.7	2.467	1.114
28/05/2019 15:45–18:35	4.9e9/1.8e6	0.06/300.69	0/0	1.8/4.18	4.232	2.454
20/07/2019 12:45–12:55	0.7e9/4e6	0.068/80	0.4/0.1	1.4/3.1	1.17	1.27
20/07/2019 13:00–14:30	5.8e9/4e6	0.063/95	0.15/0.1	1.8/2.9	5.14	1.9

**Table B1**  
*Continued*

Time interval (UT)	$j_1/j_2$	$E_1/E_2$	$\gamma_1/\gamma_2$	$\kappa_1/\kappa_2$	$n_e$ (cm <sup>-3</sup> )	$P_e$ (nPa)
01/06/2020 18:05–20:55	4e9/5e6	0.061/90	0.4/0	1.7/3.5	3.28	1.532
24/07/2020 14:25–16:55	20e9/4e6	0.037/85	0/0.15	1.7/3.1	11.431	1.715
15/09/2020 09:55–11:05	4e9/5e6	0.043/85	0.4/0.3	1.7/3.2	2.235	1.278
07/11/2020 11:15–12:25	9e9/4e6	0.025/50	0/0.2	1.6/2.7	3.756	1.049
30/12/2020 05:25–08:05	9e9/5e6	0.024/50	0.4/0	1.5/3.3	3.733	0.983
21/02/2021 01:25–04:15	5e9/5e6	0.07/50	0/0.15	1.95/2.6	4.419	1.296
15/04/2021 07:15–10:05	5e9/5e6	0.067/50	0/0.085	1.73/2.4	7.321	1.887
07/06/2021 15:25–18:15	4e9/5e6	0.066/50	0/0.08	1.68/2.35	5.836	1.863
Time interval (UT)	$j_1/j_2$	$E_1/E_2$	$\gamma_1/\gamma_2$	$\kappa_1/\kappa_2$	$n_e$ (cm <sup>-3</sup> )	$P_e$ (nPa)
07/06/2021 15:25–16:50	8e9/3.3e6	0.027/90	0/0	1.45/2.9	6.55	1.957
07/06/2021 16:50–17:00	2.7e9/1e6	0.043/75	0.4/0.5	1.5/2.6	2.94	0.618
07/06/2021 17:05–18:15	6e9/3e6	0.03/90	0.3/0	1.45/2.9	4.99	1.75
20/07/2021 15:45–18:45	3e9/5e6	0.03/20	0/0.7	1.2/2.35	5.959	1.495
02/09/2021 06:15–06:20	N/A	N/A	N/A	N/A	1.5	0.686
02/09/2021 06:20–09:10	15e9/5e6	0.048/40	0.4/0	1.9/2.35	10.501	1.373
16/10/2021 02:15–03:45	5e9/5e6	0.037/90	0/0.22	1.6/2.99	4.212	1.942
28/11/2021 22:35–00:45	16e9/5e6	0.027/80	0/0.32	1.65/2.6	11.241	2.269
11/01/2022 18:55–21:05	26e9/4.5e6	0.019/30	0/0	1.75/2	11.246	1.431
24/02/2022 09:35–12:25	9e9/5e6	0.019/30	0.7/0.65	1.55/1.7	3.085	1.986
09/04/2022 01:15–02:15	10e9/5e6	0.025/25	0.3/0.3	1.55/1.73	5.075	1.7998
22/05/2022 11:35–12:45	10e9/5e6	0.02/35	0/0.4	1.35/2.4	6.493	1.719
16/08/2022 22:35–01:15	25e9/5e6	0.0155/90	0/0.16	1.55/2.8	8.949	2.701

*Note.* Same colour code as in Table B1. The only case when Juno is below the magnetodisk is indicated in gray, but the fit to the bi-kappa distribution is not converging so no parameters are returned. All the omnidirectional fluxes  $j$  are in electrons per cm<sup>2</sup>-s-sr-keV and all the energies  $E_1$  and  $E_2$  are in keV.

### Appendix C: Summary of the Parameters of the Bi-Kappa Distributions Representing Average Electron Omnidirectional Fluxes for the Various Regions Studied

See Table C1

**Table C1**

*Values for the Parameters of the Bi-Kappa Distributions Presented in Equation 2 for the Average Electron Omnidirectional Fluxes in the Key Regions of Our Study*

Case	$j_1/j_2$	$E_1/E_2$	$\gamma_1/\gamma_2$	$\kappa_1/\kappa_2$
Within the magnetodisk	8e9/6e6	0.03/90	0/0.4	1.45/3.2
Above the magnetodisk	2.7e9/4e6	0.048/85	0.6/0.3	1.6/3
Along a complete Ganymede's orbit	4e9/4e6	0.038/85	0/0.3	1.5/3
Open field line magnetosphere of Ganymede	2.7e9/1e6	0.043/75	0.4/0.5	1.5/2.6

*Note.* All the omnidirectional fluxes  $j$  Are in electrons per cm<sup>2</sup>-s-sr-keV and all the energies  $E_1$  and  $E_2$  Are in keV.

## Appendix D: JUICE Radiation Environment Models Considered

See Table D1

**Table D1**

*Predicted Average Differential Trapped Electron Flux for the Mean JOSE Model and the GCO5000 Phase of the JUICE Mission Covering the JADE and JEDI Energy Ranges, Extracted From the JUICE Environment Specifications, JS-14-09, Version 4.9 (Table 40) and Version 5.6 (Table 19, Phase 5a)*

$E$	$j_e(\text{JOSE})$	$j_e(\text{GCO5000})$
20	1.7e5	1.64e5
30	2.27e5	2.19e5
50	1.63e5	1.58e5
70	9.43e4	9.11e4
100	5.18e4	4.89e4
200	1.68e4	1.59e4
300	8.21e3	7.77e3
500	3.97e3	3.77e3
700	2.75e3	2.6e3
1000	9.31e2	8.86e2

Note.  $j_e$  is in electrons per  $\text{cm}^2\text{-s-sr-keV}$  and the energy  $E$  is in keV.

### Data Availability Statement

The JADE and JEDI data used in this study can be found in the JNO-J-SW-JAD-3-CALIBRATED-V1.0 data set (Allegrini, 2023) and in the JNO-J-JED-3-CDR-V1.0 (Mauk, 2022) data set publicly available from the Planetary Plasma Interactions (PDS-PPI, <https://pds-ppi.igpp.ucla.edu/>) node of the Planetary Data System. The magnetic field data used for JADE pitch angles are provided in the JADE files. JEDI pitch angles are directly provided in the JEDI files. The Juno and Ganymede orbital information can be found in the corresponding spice kernels publicly available from the Navigation and Ancillary Information Facility (NAIF, <http://naif.jpl.nasa.gov>). Part of the analysis have been done with the publicly-available AMDA software (<https://amda.cdpp.eu>, Génot et al., 2021) provided by the french national data center for natural plasmas of the solar system CDPP (<https://www.cdpp.eu/>) as well as with the publicly-available CLWeb software (<http://clweb.irap.omp.eu>) developed by E. Penou at IRAP.

### References

- Achilleos, N., André, N., Blanco-Cano, X., Brandt, P. C., Delamere, P. A., & Winglee, R. (2015). Transport of mass, momentum and energy in planetary magnetodisc regions. *Space Science Reviews*, 187(1–4), 229–299. <https://doi.org/10.1007/s11214-014-0086-y>
- Allegrini, F. (2023). JNO-J-SW-JAD-5-CALIBRATED-V1.0 [Dataset]. NASA. <https://doi.org/10.17189/1519715>
- Allegrini, F., Bagenal, F., Ebert, R. W., Louarn, P., McComas, D. J., Szalay, J. R., et al. (2022). Plasma observations during the 7 June 2021 Ganymede flyby from the Jovian Auroral distributions experiment (JADE) on Juno. *Geophysical Research Letters*, 49(23), e2022GL098682. <https://doi.org/10.1029/2022GL098682>
- Allioux, R., Louarn, P., & André, N. (2013). Model of energetic populations at Ganymede, implications for an orbiter. *Advances in Space Research*, 51(7), 1204–1212. <https://doi.org/10.1016/j.asr.2012.10.033>
- Bagenal, F., & Delamere, P. A. (2011). Flow of mass and energy in the magnetospheres of Jupiter and Saturn. *Journal of Geophysical Research*, 116(A5), A05209. <https://doi.org/10.1029/2010JA016294>
- Bagenal, F., Wilson, R. J., Siler, S., Paterson, W. R., & Kurth, W. S. (2016). Survey of Galileo plasma observations in Jupiter's plasma sheet. *Journal of Geophysical Research: Planets*, 121(5), 871–894. <https://doi.org/10.1002/2016JE005009>
- Baragiola, R. A. (2003). Water ice on outer solar system surfaces: Basic properties and radiation effects. *Planetary and Space Science*, 51(14–15), 953–961. <https://doi.org/10.1016/j.pss.2003.05.007>
- Bolton, S., Lunine, J., Stevenson, D., Connerney, J., Levin, S., Owen, T., et al. (2017). The Juno mission. *Space Science Reviews*, 213(1), 5–37. <https://doi.org/10.1007/s11214-017-0429-6>
- Clark, G., Kollmann, P., Mauk, B. H., Paranicas, C., Haggerty, D., Rymer, A., et al. (2022). Energetic charged particle observations during Juno's close flyby of Ganymede. *Geophysical Research Letters*, 49(23), e2022GL098572. <https://doi.org/10.1029/2022GL098572>
- Connerney, J. E. P., Timmins, S., Oliverson, R. J., Espley, J. R., Joergensen, J. L., Kotsiaros, S., et al. (2022). A new model of Jupiter's magnetic field at the completion of Juno's prime mission. *Journal of Geophysical Research: Planets*, 127(2), e2021JE007055. <https://doi.org/10.1029/2021JE007055>
- Cooper, J. F., Johnson, R. E., Mauk, B. H., Garrett, H. B., & Gehrels, N. (2001). Energetic ion and electron irradiation of the icy Galilean satellites. *Icarus*, 149(1), 133–159. <https://doi.org/10.1006/icar.2000.6498>

### Acknowledgments

We are grateful to NASA and contributing institutions that have made the Juno mission possible. French authors acknowledge the support of Centre National d'Etudes Spatiales (CNES, France) to the Juno mission, as well as the support from CNES and from CNRS/INSU national programs of planetology (PNP) and heliophysics (PNST). S.P. and M.R. are funded by the Sun Planet Interactions Digital Environment Runs on request (SPIDER) Virtual Activity of the European Union's Horizon 2020 programme under grant agreement No 871149 for Europlanet 2024 RI. M.R. was also funded by a CNES postdoctoral fellowship. The research performed by N.A. and Q.N. holds as part of the project FACOM (ANR-22-CE49-0005-01 ACT) and has benefited from a funding provided by l'Agence Nationale de la Recherche (ANR) under the Generic Call for Proposals 2022. The work at SwRI was funded by the NASA New Frontiers Program for Juno through contract NNM06AA75C. The work at APL was funded by NASA New Frontiers Program for Juno via subcontract with the Southwest Research Institute. This work was supported at the University of Colorado as a part NASA's Juno mission supported by NASA through contract 699050X with the Southwest Research Institute.

- de Soria-Santacruz, M., Garrett, H. B., Evans, R. W., Jun, I., Kim, W., Paranicas, C., & Drozdov, A. (2016). An empirical model of the high-energy electron environment at Jupiter. *Journal of Geophysical Research: Space Physics*, *121*(10), 9732–9743. <https://doi.org/10.1002/2016JA023059>
- Ebert, R. W., Fuselier, S. A., Allegrini, F., Bagenal, F., Bolton, S. J., Clark, G., et al. (2022). Evidence for magnetic reconnection at Ganymede's upstream magnetopause during the PJ34 Juno flyby. *Geophysical Research Letters*, *49*(23), e2022GL099775. <https://doi.org/10.1029/2022GL099775>
- Evans, H. D. R., Daly, E. J., Nieminen, P., Santin, G., & Erd, C. (2013). Jovian radiation belt models, uncertainties and margins. *IEEE Transactions on Nuclear Science*, *60*(4), 2397–2403. <https://doi.org/10.1109/TNS.2013.2249097>
- Fatemi, S., Poppe, A. R., Khurana, K. K., Holmström, M., & Delory, G. T. (2016). On the formation of Ganymede's surface brightness asymmetries: Kinetic simulations of Ganymede's magnetosphere. *Geophysical Research Letters*, *43*(10), 4745–4754. <https://doi.org/10.1002/2016GL068363>
- Frank, L., Ackerson, K., Lee, J., English, M., & Pickett, G. (1992). The plasma instrumentation for the Galileo mission. *Space Science Reviews*, *60*(1–4), 283–304. <https://doi.org/10.1007/BF00216858>
- Garrett, H. B., Jun, I., Ratliff, J., Evans, R., Clough, G., & McEntire, R. (2003). *Status of Galileo interim radiation electron model*. JPL Publication.
- Génot, V., Budnik, E., Jacquy, C., Bouchemit, M., Renard, B., Dufourg, N., et al. (2021). Automated Multi-Dataset Analysis (AMDA): An online database and analysis tool for heliospheric and planetary plasma data. *Planetary and Space Science*, *201*, 105214. <https://doi.org/10.1016/j.pss.2021.105214>
- Grasset, O., Dougherty, M., Coustenis, A., Bunce, E., Erd, C., Titov, D., et al. (2013). Jupiter ICy moons Explorer (JUICE): An ESA mission to orbit Ganymede and to characterise the Jupiter system. *Planetary and Space Science*, *78*, 1–21. <https://doi.org/10.1016/j.pss.2012.12.002>
- Haggerty, D. K., Mauk, B. H., Paranicas, C. P., Clark, G., Kollmann, P., Rymer, A. M., et al. (2019). Jovian injections observed at high latitude. *Geophysical Research Letters*, *46*(16), 9397–9404. <https://doi.org/10.1029/2019GL083442>
- Hawkins III, S. E., Cheng, A. F., & Lanzerotti, L. J. (1998). Bulk flows of hot plasma in the Jovian magnetosphere: A model of anisotropic fluxes of energetic ions. *Journal of Geophysical Research*, *103*(E9), 20031–20054. <https://doi.org/10.1029/98JE01253>
- Jun, I., Garrett, H. B., Cassidy, T. A., Kim, W., & Dougherty, L. (2019). Updating the Jovian electron plasma environment. *IEEE Transactions on Plasma Science*, *47*(8), 3915–3922. <https://doi.org/10.1109/TPS.2019.2901681>
- Jun, I., Garrett, H. B., Swimm, R., Evans, R. W., & Clough, G. (2005). Statistics of the variations of the high-energy electron population between 7 and 28 Jovian radii as measured by the Galileo spacecraft. *Icarus*, *178*(2), 386–394. <https://doi.org/10.1016/j.icarus.2005.01.022>
- Khurana, K. K., Leinweber, H. K., Hospodarsky, G. B., & Paranicas, C. P. (2022). Radial and local time variations in the thickness of Jupiter's magnetospheric current sheet. *Journal of Geophysical Research: Space Physics*, *127*(10), e2022JA030664. <https://doi.org/10.1029/2022JA030664>
- Khurana, K. K., Pappalardo, R. T., Murphy, N., & Denk, T. (2007). The origin of Ganymede's polar caps. *Icarus*, *191*(1), 193–202. <https://doi.org/10.1016/j.icarus.2007.04.022>
- Kivelson, M. G., Bagenal, F., Kurth, W. S., Neubauer, F. M., Paranicas, C., & Saur, J. (2004). Magnetospheric interactions with satellites. *Jupiter: The Planet, Satellites and Magnetosphere*, *1*, 513–536.
- Krimigis, S. M., Carbary, J. F., Keath, E. P., Bostrom, C. O., Axford, W. I., Gloeckler, G., et al. (1981). Characteristics of hot plasma in the Jovian magnetosphere: Results from the Voyager spacecraft. *Journal of Geophysical Research*, *86*(A10), 8227–8257. <https://doi.org/10.1029/JA086iA10p08227>
- Krupp, N., Woch, J., Lagg, A., Livi, S., Mitchell, D. G., Krimigis, S. M., et al. (2004). Energetic particle observations in the vicinity of Jupiter: Cassini MIMI/LEMMS results. *Journal of Geophysical Research*, *109*(A9), A09S10. <https://doi.org/10.1029/2003JA010111>
- Leblanc, F., Oza, A., Leclercq, L., Schmidt, C., Cassidy, T., Modolo, R., et al. (2017). On the orbital variability of Ganymede's atmosphere. *Icarus*, *293*, 185–198. <https://doi.org/10.1016/j.icarus.2017.04.025>
- Leblanc, F., Roth, L., Chaufray, J., Modolo, R., Galand, M., Ivchenko, N., et al. (2023). Ganymede's atmosphere as constrained by HST/STIS observations. *Icarus*, *399*, 115557. <https://doi.org/10.1016/j.icarus.2023.115557>
- Liuzzo, L., Poppe, A. R., Paranicas, C., Nénon, Q., Fatemi, S., & Simon, S. (2020). Variability in the energetic electron bombardment of Ganymede. *Journal of Geophysical Research: Space Physics*, *125*(9), e2020A028347. <https://doi.org/10.1029/2020A028347>
- Ma, Q., Li, W., Zhang, X.-J., Shen, X.-C., Daly, A., Bortnik, J., et al. (2021). Energetic electron distributions near the magnetic equator in the Jovian plasma sheet and outer radiation belt using Juno observations. *Geophysical Research Letters*, *48*(24), e2021GL095833. <https://doi.org/10.1029/2021GL095833>
- Mauk, B. (2022). JEDI CALIBRATED (CDR) DATA JNO J JED 3 CDR V1.0 [Dataset]. NASA. <https://doi.org/10.17189/1519713>
- Mauk, B. H., Clark, G., Gladstone, G. R., Kotsiaros, S., Adriani, A., Allegrini, F., et al. (2020). Energetic particles and acceleration regions over Jupiter's polar cap and main aurora: A broad overview. *Journal of Geophysical Research: Space Physics*, *125*(3), e2019JA027699. <https://doi.org/10.1029/2019JA027699>
- Mauk, B. H., Gary, S. A., Kane, M., Keath, E. P., Krimigis, S. M., & Armstrong, T. P. (1996). Hot plasma parameters of Jupiter's inner magnetosphere. *Journal of Geophysical Research*, *101*(A4), 7685–7695. <https://doi.org/10.1029/96JA00006>
- Mauk, B. H., Haggerty, D., Jaskulek, S., Schlemm, C., Brown, L., Cooper, S., et al. (2017). The Jupiter energetic particle detector instrument (JEDI) investigation for the Juno mission. *Space Science Reviews*, *213*(1–4), 289–346. <https://doi.org/10.1007/s11214-013-0025-3>
- Mauk, B. H., Szalay, J. R., Allegrini, F., Bagenal, F., Bolton, S. J., Clark, G., et al. (2023). How bi-modal are Jupiter's main aurora zones? *Journal of Geophysical Research: Space Physics*, *128*(4), e2022JA031237. <https://doi.org/10.1029/2022JA031237>
- Mauk, B. H., Williams, D. J., McEntire, R. W., Khurana, K. K., & Roederer, J. G. (1999). Storm-like dynamics of Jupiter's inner and middle magnetosphere. *Journal of Geophysical Research*, *104*(A10), 22759–22778. <https://doi.org/10.1029/1999JA900097>
- McComas, D., Alexander, N., Allegrini, F., Bagenal, F., Beebe, C., Clark, G., et al. (2017). The Jovian auroral distributions experiment (JADE) on the Juno mission to Jupiter. *Space Science Reviews*, *213*(1), 547–643. <https://doi.org/10.1007/s11214-013-9990-9>
- Nénon, Q., Miller, L. P., Kollmann, P., Liuzzo, L., Pinto, M., & Witasse, O. (2022). Pitch angle distribution of MeV electrons in the magnetosphere of Jupiter. *Journal of Geophysical Research: Space Physics*, *127*(8), e2022JA030627. <https://doi.org/10.1029/2022JA030627>
- Paranicas, C., Mauk, B. H., Kollmann, P., Clark, G., Haggerty, D. K., Westlake, J., et al. (2022). Energetic charged particle fluxes relevant to Ganymede's polar region. *Geophysical Research Letters*, *49*(23), e2022GL098077. <https://doi.org/10.1029/2022GL098077>
- Paranicas, C., Paterson, W. R., Cheng, A. F., Mauk, B. H., McEntire, R. W., Frank, L. A., & Williams, D. J. (1999). Energetic particle observations near Ganymede. *Journal of Geophysical Research*, *104*(A8), 17459–17469. <https://doi.org/10.1029/1999JA900199>
- Paranicas, C., Szalay, J. R., Mauk, B. H., Clark, G., Kollmann, P., Haggerty, D. K., et al. (2021). Energy spectra near Ganymede from Juno data. *Geophysical Research Letters*, *48*(10), e2021GL093021. <https://doi.org/10.1029/2021GL093021>

- Paschmann, G., Fazakerley, A. N., & Schwartz, S. J. (1998). Moments of plasma velocity distributions. Analysis methods for multi spacecraft data. *ISSI, I*, 125–157.
- Phipps, P., & Bagenal, F. (2021). Centrifugal equator in Jupiter's plasma sheet. *Journal of Geophysical Research: Space Physics*, 126(1), e2020JA028713. <https://doi.org/10.1029/2020JA028713>
- Plainaki, C., Massetti, S., Jia, X., Mura, A., Roussos, E., Milillo, A., & Grassi, D. (2022). The Jovian energetic ion environment of Ganymede: Planetary space weather considerations in view of the JUICE mission. *The Astrophysical Journal*, 940(2), 186. <https://doi.org/10.1016/j.icarus.2014.09.018>
- Plainaki, C., Milillo, A., Massetti, S., Mura, A., Jia, X., Orsini, S., et al. (2015). The H<sub>2</sub>O and O<sub>2</sub> exospheres of Ganymede: The result of a complex interaction between the Jovian magnetospheric ions and the icy moon. *Icarus*, 245, 306–319. <https://doi.org/10.1016/j.icarus.2014.09.018>
- Poppe, A. R., Fatemi, S., & Khurana, K. K. (2018). Thermal and energetic ion dynamics in Ganymede's magnetosphere. *Journal of Geophysical Research: Space Physics*, 123(6), 4614–4637. <https://doi.org/10.1029/2018JA025312>
- Schaible, M., Johnson, R., Zhigilei, L., & Piqueux, S. (2017). High energy electron sintering of icy regoliths: Formation of the PacMan thermal anomalies on the icy Saturnian moons. *Icarus*, 285, 211–223. <https://doi.org/10.1016/j.icarus.2016.08.033>
- Scudder, J. D., Sittler, E. C., Jr., & Bridge, H. S. (1981). A survey of the plasma electron environment of Jupiter: A view from Voyager. *Journal of Geophysical Research*, 86(A10), 8157–8179. <https://doi.org/10.1029/JA086iA10p08157>
- Sicard-Piet, A., Bourdarie, S., & Krupp, N. (2011). JOSE: A new Jovian specification environment model. *IEEE Transactions on Nuclear Science*, 58(3), 923–931. <https://doi.org/10.1109/TNS.2010.2097276>
- Tomás, A., Woch, J., Krupp, N., Lagg, A., Glassmeier, K.-H., Dougherty, M., & Hanlon, P. (2004). Changes of the energetic particles characteristics in the inner part of the Jovian magnetosphere: A topological study. *Planetary and Space Science*, 52(5), 491–498. <https://doi.org/10.1016/j.pss.2003.06.011>
- Trumbo, S. K., Brown, M. E., Bockelée-Morvan, D., de Pater, I., Fouchet, T., Wong, M. H., et al. (2023). Hydrogen peroxide at the poles of Ganymede. *Science Advances*, 9(29), eadg3724. <https://doi.org/10.1126/sciadv.adg3724>
- Valek, P. W., Waite, J. H., Allegrini, F., Ebert, R. W., Bagenal, F., Bolton, S. J., et al. (2022). In situ ion composition observations of Ganymede's outflowing ionosphere. *Geophysical Research Letters*, 49(24), e2022GL100281. <https://doi.org/10.1029/2022GL100281>
- van Allen, J. A. (1979). Energetic electrons in Jupiter's dawn magnetodisc. *Geophysical Research Letters*, 6(4), 309–312. <https://doi.org/10.1029/g1006i004p00309>
- Vogt, M. F., Bagenal, F., & Bolton, S. J. (2022). Magnetic field conditions upstream of Ganymede. *Journal of Geophysical Research: Space Physics*, 127(12), e2022JA030497. <https://doi.org/10.1029/2022JA030497>
- Vorburger, A., Fatemi, S., Galli, A., Liuzzo, L., Poppe, A. R., & Wurz, P. (2022). 3D Monte-Carlo simulation of Ganymede's water exosphere. *Icarus*, 375, 114810. <https://doi.org/10.1016/j.icarus.2021.114810>
- Williams, D., McEntire, R., Jaskulek, S., & Wilken, B. (1992). The Galileo energetic particles detector. *Space Science Reviews*, 60(1–4), 385–412. <https://doi.org/10.1007/BF00216863>